# A Novel Timing Recovery Algorithm for Digital Multi-Band Systems with Enhanced DPLL Performance

Wanzhen Guo(1), Ziheng Zhang(1), Jiating Luo(2), Bofang Zheng(2), and Jian Zhao(1)

(1) School of Electronic and Information Engineering, South China University of Technology, Guangzhou, China, zhaojian@scut.edu.cn
(2) Huawei Technologies Co. Ltd., Shenzhen, China

**Abstract** *We propose a novel timing recovery algorithm for digital multi-band systems. 320-Gbit/s experiments show that the proposed algorithm is robust to spectral roll-off, dispersion and DGD and outperforms the double-period algorithm under large clock frequency offsets and loop delays.* *©2023 The Author(s)*

## Introduction

Timing recovery (TR) is essential for long-haul transmission. In TR, timing error (TE) is extracted by the timing recovery algorithm (TRA) and fed back to adjust the clock sampling phase. Gardner and Godard TRAs [1-4] have been widely used in QAM formats due to their simplicity. However, these two methods do not work for QAM signals with a small spectral roll-off. A square-Gardner (sGardner) method [5] was proposed to enhance the tolerance to the spectral roll-off. However, all these methods fail when the differential group delay (DGD) is equal to half of the symbol period and are also inapplicable to offset quadrature amplitude modulation (OQAM) format [6].

Recently, we proposed a pilot-aided TRA, named double-period algorithm (DPA), for OQAM-based digital multi-band (DMB) [6]. DPA is robust to different impairments, especially the spectral roll-off and DGD which traditional methods are sensitive to. However, the S-curve of the DPA is a double-period sine function, which affects the convergence of the digital phase-lock loop (DPLL) under a large clock frequency offset (CFO) or a large loop delay.

In this paper, we propose a novel pilot-aided TRA which outperforms DPA under large CFOs or loop delays. 320-Gbit/s experiments show that OQAM-DMB based on the proposed method exhibits a negligible penalty for all spectral roll-offs and DGDs and outperforms QAM-DMB using traditional TRAs. Particularly, the DPLL can be locked for CFOs within ±160 ppm and loop delays within 64 ns, twice of those of DPA. It is also shown that the proposed method can be applied to QAM-DMB.

## Principle

Fig. 1 shows OQAM-DMB with 4 subbands. In [6], we have proved that by multiplying the pilots in subband A with the conjugate of the pilots in subband B, we can extract TE $\tau$ and eliminate the effects of residual dispersion, phase noise and carrier frequency offset. In this paper, we still use subbands A and B to extract TE and the design of the pilot symbols is shown in Tab. 1.

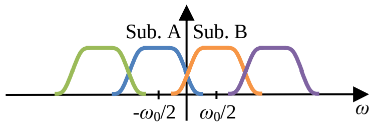


**Fig. 1:** Diagram of OQAM-DMB subbands. $\omega_0 = 2\pi/T$ and $T$ is the symbol period of a subband.

**Tab. 1:** Design of pilot symbols.

| | Odd pilots | Even pilots |
|---|---|---|
| x-pol | $P_x$ | $-P_y^*$ |
| y-pol | $P_y$ | $P_x^*$ |

However, the amplitude of TE will be affected by the rotation of state of polarization (RSOP) and DGD. In this paper, we propose a novel TRA, called the complementary algorithm (CA), which uses two complementary metrics to cover all SOP and DGD and also enhances the tolerance of the DPLL to the CFO and loop delay.

The signals of x- and y- polarization in subbands A and B after demultiplexing, $X_{A/B,out}(t)$ and $Y_{A/B,out}(t)$, can be derived as:

$$\begin{bmatrix} X_{A/B,out}(t) \\ Y_{A/B,out}(t) \end{bmatrix} = h_{A/B}(t) \otimes \begin{bmatrix} X_{A/B,in}(t-\tau)\cdot\exp(j\omega_0\tau/2) \\ Y_{A/B,in}(t-\tau)\cdot\exp(-j\omega_0\tau/2) \end{bmatrix} \quad (1)$$

where $X_{A/B,in}(t)$ and $Y_{A/B,in}(t)$ are the signals before multiplexing at the transmitter. $\otimes$ is the convolution operator. $h_{A/B}(t)$ are the Jones matrices of subbands A and B, whose frequency-domain representations are:

$$H_A(\omega) = R_1 Q \begin{bmatrix} e^{j(\omega-\omega_0/2)\tau_D} & 0 \\ 0 & e^{-j(\omega-\omega_0/2)\tau_D} \end{bmatrix} Q^{-1} R_2 \quad (2\text{-}1)$$

$$H_B(\omega) = R_1 Q \begin{bmatrix} e^{j(\omega+\omega_0/2)\tau_D} & 0 \\ 0 & e^{-j(\omega+\omega_0/2)\tau_D} \end{bmatrix} Q^{-1} R_2 \quad (2\text{-}2)$$

where $2\tau_D$ is the DGD, $R_i$ and $Q$ are unity matrices:

$$R_i = \begin{bmatrix} \cos\varphi_i & -\sin\varphi_i \\ \sin\varphi_i & \cos\varphi_i \end{bmatrix},\ Q = \begin{bmatrix} \cos\varphi_3 & \sin\varphi_3 e^{-j\theta} \\ -\sin\varphi_3 e^{j\theta} & \cos\varphi_3 \end{bmatrix} \quad (3)$$

We first perform correlation to locate and align the pilots for subbands A and B. By using the design in Tab. 1, the correlation functions of the pilot waveforms are symmetric, allowing for identification of the waveforms and their center of symmetry (CoS). We define the odd and even pilot waveforms of x- and y-polarization after demultiplexing at the receiver are $A_{x,odd}$, $A_{x,even}$, $A_{y,odd}$, $A_{y,even}$ for subband A, and $B_{x,odd}$, $B_{x,even}$, $B_{y,odd}$, $B_{y,even}$ for subband B. The proposed algorithm includes two metrics:

$$SA_1 = j\cdot(A_{x,odd}B^{\dagger}_{y,odd} - A'_{y,odd}B^{*}_{x,odd} - A_{x,even}B^{\dagger}_{y,even} + A'_{y,even}B^{*}_{x,even} + A'_{x,odd}B^{*}_{y,odd} - A_{y,odd}B^{\dagger}_{x,odd} - A'_{x,even}B^{*}_{y,even} + A_{y,even}B^{\dagger}_{x,odd}) \quad (4\text{-}1)$$

$$SA_2 = \sqrt{(A_{x,odd}B^{*}_{x,odd} + A_{y,odd}B^{*}_{y,odd})(A'_{x,even}B^{\dagger}_{x,even} + A'_{y,even}B^{\dagger}_{y,even})} \quad (4\text{-}2)$$

where $(\cdot)^*$ denotes the conjugate operator, $(\cdot)'$ is to flip the waveform about the CoS, and $(\cdot)^\dagger$ represents flipping the waveform about CoS and conjugating it.

From Eqs. (1)-(4), we get

$$SA_1 = \eta_1 \cdot \exp(j\omega_0\tau) \quad (5\text{-}1)$$

$$SA_2 = \sqrt{\eta_2} \cdot \exp(j\omega_0(\tau \pm \pi)) \quad (5\text{-}2)$$

where $\eta_1$ and $\eta_2$ are real values:

$$\eta_1 = \left(2\cdot \mathrm{Im}\left\{U_1^{\,2}X_1Y_1 - U_2^{\,2}X_1^{\,*}Y_1^{\,*}\right\}\right)\cdot\left(h^2(t+\tau_D)+h^2(t-\tau_D)\right) + 8\cdot \mathrm{Im}\{U_1U_2\}\left(|X_1|^2 - |Y_1|^2\right)\cos(\omega_0\tau_D)h(t+\tau_D)h(t-\tau_D) \quad (6\text{-}1)$$

$$\eta_2 = |X_1|^4 h^4(t+\tau_D) + |Y_1|^4 h^4(t-\tau_D) + 2|X_1|^2|Y_1|^2 h^2(t+\tau_D)h^2(t-\tau_D)\cos(2\omega_0\tau_D) \quad (6\text{-}2)$$

in which $[X_1, -Y_1^*]^{\mathrm{T}} = Q^{-1}R_2[P_x, P_y]^{\mathrm{T}}$, $h(t)$ is the shaping pulse and

$$\begin{bmatrix} U_1 & U_2 \\ -U_2^* & U_1^* \end{bmatrix} = R_1Q \quad (7)$$

From Eq. (5), because $\eta_1$ and $\eta_2$ are real, the TE can be extracted from the phase of $SA_1$ or $SA_2$. Although the values of $\eta_1$ and $\eta_2$ and their SNRs change with the SOP and DGD, it can be proved that the optimum working conditions of $SA_1$ and $SA_2$ are opposite. That is, for any SOP and DGD, there is at least one metric that has a good SNR to extract the TE. Therefore, by combining the two metrics, we can cover all situations of SOP and DGD. In order to decide which metric is used, we evaluate the SNRs of the two metrics as:

$$\mathrm{SNR}_i = 10\log_{10}\left(|SA_i|/P_{noise}\right), i = 1, 2 \quad (8)$$

in which $P_{noise}$ is the noise power nearby the pilots.

In Eq. (5-2), the TE obtained by $SA_2$ has a $\pi$ phase ambiguity. This can be removed by utilizing the phases in $A_{x,odd}B^*_{x,odd} + A_{y,odd}B^*_{y,odd}$ and $A'_{x,even}B^{\dagger}_{x,even} + A'_{y,even}B^{\dagger}_{y,even}$. The S-curve of the proposed CA is a single-period sine curve, which is expected to enhance the performance of DPLL.

## Experimental setup and results

Fig. 2 shows the experimental setup of a 40-Gbaud DMB system with DP-16OQAM or DP-16QAM format. The roll-off factor was 0.1 unless specified. Pilot symbols were inserted into payload symbols periodically at a ratio of 1/32 with $P_x$ = 3+3j and $P_y$ = 3-3j. SMF was used to investigate the influence of residual dispersion. After a PC, the signal was split into two polarizations, whose delays were controlled by PM-VODL1 and PM-VODL2 to emulate the DGD. Then, PBC was used to combine the two signals. OSNR was set to be 24 dB by adjusting VOA1 and the received power was set to -7 dBm. In the receiver DSP, as shown in Fig. 3, TE was first added to emulate the CFO and initial sampling phase offset. The signal with TE was demultiplexed into subbands. Subbands A and B as described in Fig. 1 were used to calculate the $SA_1$ and $SA_2$, and the one with a higher SNR was used to control the digital oscillator. A loop delay of 12.8 ns was added unless specified. The BER was measured after the DPLL had been locked.

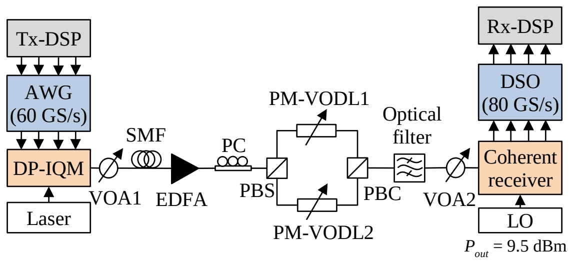


**Fig. 2:** Experimental setup. AWG: arbitrary waveform generator; DP-IQM: dual-polarization IQ modulator; VOA: variable optical attenuator; SMF: single mode fiber; PC: polarization controller; PM-VODL: polarization-maintaining variable optical delay line; PBS/PBC: polarization beam splitter/combiner; DSO: digital storage oscilloscope.

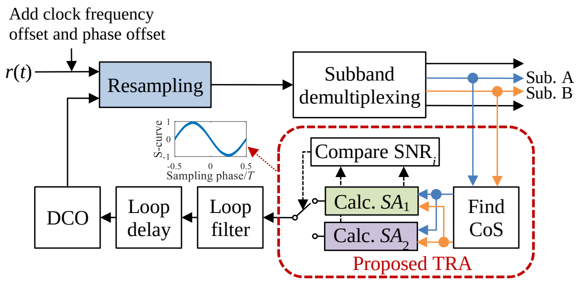


**Fig. 3:** Structure of the digital phase-lock loop. CoS: center of symmetry; DCO: digitally controlled oscillator. Loop delay is used to emulate the hardware delay. Insert: S-curve of CA. $SA_1$ and $SA_2$ are complementary to cover all RSOP and DGD.

Fig. 4 depicts the BER versus DGD for OQAM-DMB using the proposed TRA at back-to-back and with 5-km dispersion. At back-to-back, the PC was adjusted to change the SOP of the signal and the results for three random SOPs are given. It is seen that the proposed CA works properly with a negligible penalty for up to 2*T* DGD. Fig. 5 (a) and (b) show the SNR curves of $SA_1$ and $SA_2$ of SOP2 and SOP3, respectively. In SOP2, $\mathrm{SNR}_1>\mathrm{SNR}_2$, so $SA_1$ is selected to correct the TE. In SOP3, $SA_2$ is selected. Fig. 5 (c) and (d) shows the DPLL converges in both cases. Other SOPs were also tested and the proposed CA all works.

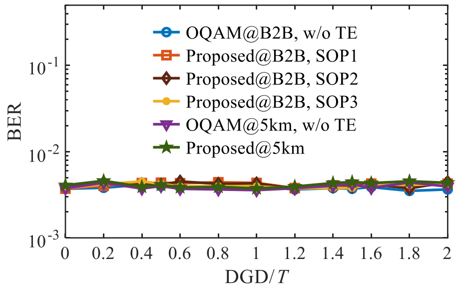


**Fig. 4:** BER versus the DGD for OQAM-DMB using the proposed TRA. The clock phase and frequency offset are *T*/6 and 20 ppm, respectively.

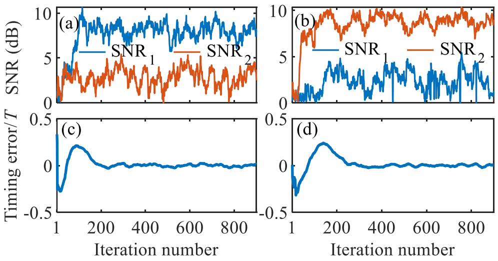


**Fig. 5:** SNR of $SA_1$ and $SA_2$ with (a) SOP2 and 0.5*T* DGD; and (b) SOP3 and 1.5*T* DGD. (c) and (d) are the corresponding convergence curves of DPLL of (a) and (b), respectively.

Fig. 6 shows the BER versus the roll-off factor for OQAM-DMB using the proposed CA. Traditional TRAs were investigated in QAM-DMB for comparison because they fail in OQAM-DMB. Note the bandwidth of QAM-DMB increases with the roll-off factor due to the guard band. It is seen that OQAM-DMB using the proposed method has outstanding performance for all roll-off factors, while QAM-DMB using traditional TRAs is sensitive to the roll-off factor.

Fig. 7 compares the CFO tolerance of CA and DPA in OQAM-DMB. Because the S-curve of the proposed CA has single period in [-0.5*T*, 0.5*T*] while that of DPA has two periods, CA can tolerate CFO within ±160ppm, double that of DPA. The characteristic of S-curve also affects the tolerance of DPLL to the loop delay. As shown in Fig. 8, the loop delay tolerance of the proposed CA is 64 ns when the CFO is ±60 ppm, while that of the DPA is only 32 ns. When the CFO is ±100 ppm, CA can tolerate a 44.8-ns loop delay.

The proposed method can also be applied to QAM-DMB. Fig. 9 depicts the BER versus the DGD for QAM-DMB. The proposed method exhibits a negligible penalty and solves the problem that traditional TRAs fail when the DGD equals odd times of half-symbol period.

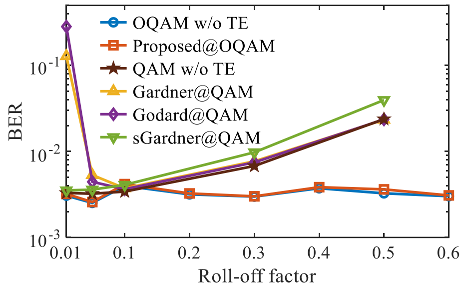


**Fig. 6:** BER of OQAM-DMB using the proposed method and QAM-DMB based on conventional methods.

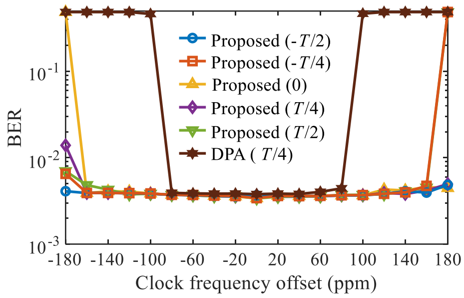


**Fig. 7:** BER versus clock frequency offset under 0.5*T* DGD. (*T*/2) etc. represent the initial sampling phase offset.

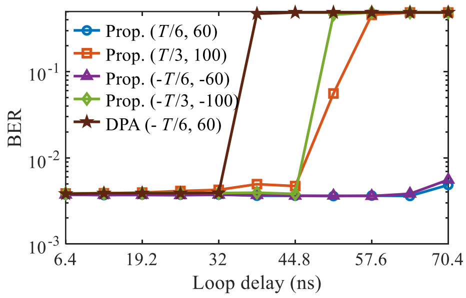


**Fig. 8:** BER versus loop delay under 0.5*T* DGD. (*T*/6, 60) etc. represent the initial sampling phase offset and CFO. The unit of CFO is ppm. Proposed is abbreviated as Prop..

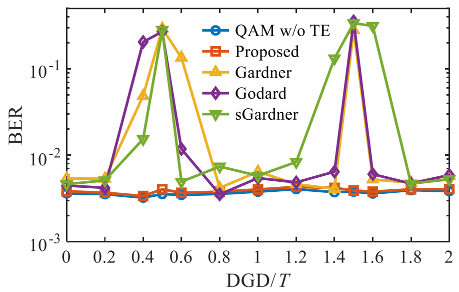


**Fig. 9:** BER versus the DGD for QAM-DMB. The clock phase and frequency offset are *T*/6 and 20 ppm, respectively.

## Conclusions

We have proposed a novel TRA and shown in 320-Gbit/s DMB experiments that the proposed CA doubles the CFO and loop delay tolerance compared to DPA and is also robust to the spectral roll-off, dispersion and DGD.

## Acknowledgments

The National Key Research and Development Program of China (2022YFB2903000) and National Natural Science Foundation of China (61971199).

## References


[1] D. Godard, "Passband timing recovery in an all-digital modem receiver," *IEEE Transactions on Communications*, vol. 26, no. 5, pp. 517-523, 1978. DOI: 10.1109/TCOM.1978.1094107.

[2] F. Gardner, "A BPSK/QPSK timing-error detector for sampled receivers," *IEEE Transactions on Communications*, vol. 34, no. 5, pp. 423-429, 1986. DOI: 10.1109/TCOM.1986.1096561.

[3] Arne Josten, Benedikt Bäeuerle, Edwin Dornbierer, Jonathan Boesser, David Hillerkuss, and Juerg Leuthold, "Modified Godard timing recovery for non-Integer oversampling receivers," *Applied Science*, vol. 7, no. 7, pp. 655-668, 2017. DOI: 10.3390/app7070655.

[4] Fabio A. Barbosa, Sandro M. Rossi, and Darli A. A. Mello, "Clock recovery limitations in probabilistically shaped transmission," *Optical Fiber Communication Conference* (*OFC*), paper M4J.4, 2020. DOI: 10.1364/OFC.2020.M4J.4.

[5] M. Yan, Z. Tao, L. Dou, L. Li, Y. Zhao, T. Hoshida, and J. C. Rasmussen, "Digital clock recovery algorithm for Nyquist signal," *Optical Fiber Communication Conference* (*OFC*), paper OTu2I.7, 2013. DOI: 10.1364/ofc.2013.otu2i.7.

[6] W. Guo, Z. Fan, Z. Zhang, J. Luo, B. Zheng and J. Zhao, "Robust pilot-aided timing recovery algorithm for OQAM-based digital multi-band systems," *European Conference on Optical Communication* (ECOC), paper Th1C.3, 2022.